Nonlinear Rotordynamics of Automotive Turbochargers: Predictions and Comparisons to Test Data

Luis San Andrés
e-mail: lsanandres@mengr.tamu.edu

Juan Carlos Rivadeneira

Mechanical Engineering Department,
Texas A&M University,
College Station, TX 77843

Murali Chinta
Honeywell Turbo Technologies,
Torrance, CA 90505

Kostandin Gjika
Honeywell Turbo Technologies,
88155 Thaon les Vosges, France

Gerry LaRue
Honeywell Turbo Technologies,
Torrance, CA 90905

Passenger vehicle turbochargers (TCs) offer increased engine power and efficiency in an ever-competitive marketplace. Turbochargers operate at high rotational speeds and use engine oil to lubricate fluid-film-bearing supports (radial and axial). However, TCs are prone to large amplitudes of subsynchronous shaft motion over wide ranges of their operating speed. Linear rotordynamic tools cannot predict the amplitudes and multiple frequency shaft motions. A comprehensive nonlinear rotordynamics model coupled to a complete fluid-film-bearing model solves in real time the dynamics of automotive turbochargers. The computational design tool predicts the limit cycle response for several inner and outer film clearances and operating conditions including rotor speed and lubricant feed pressure. Substantial savings in product development and prototype testing are the benefits of the present development. The paper presents predictions of the linear and nonlinear shaft motion of an automotive turbocharger supported on a semi-floating ring bearing. The shaft motion predictions are compared to measurements of shaft motion at the compressor nose for speeds up to 240 krpm*, and for lubricant inlet pressure of* 4 bar *at* 150°C. *Linear and nonlinear rotordynamic models reproduce very well the test data for synchronous response to imbalance. The nonlinear results show two subsynchronous whirl frequencies whose large magnitudes agree well with the measurements. A large side load predicted for this turbocharger must be considered for accurate prediction of the rotordynamic response.* [DOI: 10.1115/1.2204630]

Introduction

Most commercial automotive turbochargers incorporate engine oil lubricated floating ring bearings (FRBs) due to their low cost and reduced power losses [1,2]. Passenger vehicles TCs are more compact units that implement semi-floating ring bearings (SFRBs) with integral thrust bearings. FRBs comprise two fluid films in series with the ring spinning at a fraction of shaft speed. SFRBs are similar, except that the floating ring is pinned to prevent its rotation; thus, the outer film acts as a squeeze film damper. In [3], turbochargers supported on SFRBs have shown less power loss (~28%) than those utilizing FRBs with identical clearances, thus making more power available to drive the compressor or a lower requirement from the turbine, resulting in lower back pressure on the engine.

Persistent subsynchronous motions are present in rotor-bearing systems with a fully floating ring design, albeit reaching limit cycles that enable their continuous operation [2,4,5]. The lubricated bearings with inner and outer films acting in series are the source of the rotordynamic instabilities [6–8]. The dynamic response of lubricated TCs is thus highly nonlinear. The amplitudes and frequency content of the sub synchronous motions cannot be predicted using conventional linear rotordynamics tools [9–11]. More often, however, simple linear rotor-bearing models predict instability regions over wide operating speed ranges; while test measurements demonstrate stable performance due to a number of effects not accounted in the simple analysis. The uncertainty in actual rotor imbalance levels as well as thermal effects affecting the lubricant viscosity and actual film clearances are a few notable factors (see, for example, [2,4]). Due to the lack of accurate and efficient predictive tools, turbocharger rotordynamic design followed, until recently, costly test stand iteration [12,13].

The demand for maximum turbocharger speed and variable geometry technology continues to increase, thus requiring the development of lighter materials with higher strengths. Bearing systems in automotive turbochargers currently perform under extreme operating conditions with attendance to stringent environmental considerations. Present applications use low viscosity (light) lubricants delivered at high operating temperatures (up to 150°C) and with reduced feed pressures [14]. In 2000, a prominent turbomachinery manufacturer along with a university research laboratory initiated an ambitious research program to develop physical models and fast computational programs to reliably predict the nonlinear rotordynamic performance of passenger and commercial vehicle turbochargers. The ultimate goal is to deliver an experimentally validated design tool that accounts for the actual operating conditions in turbochargers, including accurate modeling of the forced response of the fluid film bearings and full integration with a comprehensive rotordynamics response program. Substantial savings in product development and prototype testing are the major expected benefits.

Within the scope of the project outlined above, Naranjo et al. [15] introduced the rudiments of FRB analysis along with experimental validation in a low speed test rotor. Later, Holt et al. [16–18] present a complete nonlinear rotordynamics model and comprehensive measurements of casing acceleration in a high speed TC unit supported on FRBs. The experiments show the effects of increasing lubricant inlet pressure and temperature on the complex TC dynamic response for shaft speeds to 100 krpm. The nonlinear rotor model incorporating the FRB reaction forces in the numerical integration of the rotor equations of motion predicts the limit cycle amplitudes with two fundamental subsynchronous whirl frequencies. The predictions, validated by the test data,

Contributed by the International Gas Turbine Institute (IGTI) of ASME for publication in the JOURNAL OF ENGINEERING FOR GAS TURBINES AND POWER. Manuscript received August 25, 2005; final manuscript received September 28, 2005. IGTI Review Chair: K. C. Hall. Paper presented at the ASME Turbo Expo 2005: Land, Sea, and Air, Reno, NV, June 6–9, 2005, Paper No. GT2005-68177.

evidence two (unstable) whirl ratios at approximately one-half ring speed and one-half ring speed plus one-half journal speed. The transient nonlinear responses reveal the importance of rotor imbalance in suppressing the subsynchronous instabilities at large rotor speeds as also observed in the experiments.

Kerth and San Andrés [19] present the flow model for prediction of FRB forced response—linear and nonlinear. This model incorporates a lumped parameter thermal energy balance for estimation of the lubricant viscosity and thermal growth of the rotor, bearing and floating ring. The FRB model, fully integrated into the nonlinear rotordynamics computational program, predicts the floating ring speed, journal and ring eccentricities, power loss, and the inner and outer films' rotordynamic force coefficients as a function of the load applied at a given rotor speed. Knowledge of the actual load conditions—static and dynamic—and the changes in operating clearance and effective lubricant viscosity are of utmost importance to estimate accurately the dynamic forced response of turbochargers. In [19], predictions for the exit lubricant temperature, power losses, and floating ring speeds agree well with measurements obtained in an automotive turbocharger test rig.

References [18,19] include extensive literature reviews of the prior art in turbocharger dynamics analysis and modeling of FRBs, along with test programs attempting to validate model predictions. Analyses based on linearized bearing force coefficients have been, for the most part, unsuccessful since the actual nonlinear TC response, i.e., limit cycle amplitudes and subsynchronous frequencies, cannot be predicted. Nonetheless, linearized analyses for simple rotor-bearing systems (e.g., [5–8]), do offer insight into the intricate response of turbochargers, rich in subsynchronous motions. The present computational development, based on the time-marching numerical integration of the rotor-bearing nonlinear equations of motion, continues earlier work given in [10,11]. The computer program, emulating a virtual laboratory for evaluation of rotor-bearing systems dynamic performance, is relatively fast due to the significant advances in high processing computer technology. The application to semi-floating rotor-bearing system of a passenger car turbocharger shows good correlation between predicted and measured steady-state shaft motions. The predictive tool can be used to design high performance products with faster product development cycle times and increased product reliability.

Test Turbocharger and Measurements

Figure 1 depicts a photograph of the test turbocharger rotor and its semi-floating ring bearing (SFRB) support. The small rotor is comprised of a long and thin shaft with one end welded to the turbine wheel. The other shaft end is threaded for installation of the compressor wheel, pushing the thrust collar towards the shaft shoulder. The turbine and compressor are made of high structural

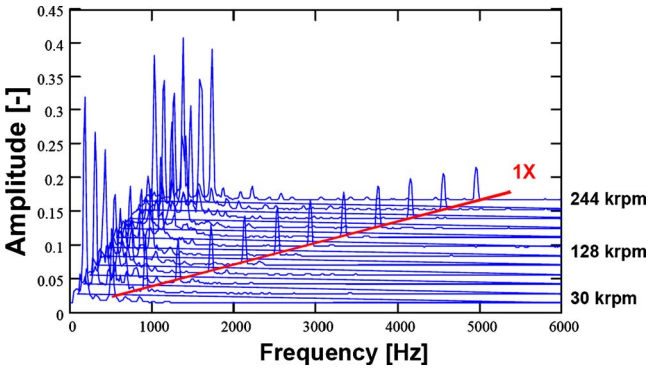

Fig. 2 Waterfall of turbocharger measured shaft displacement versus frequency. Shaft speed ranges from 29.7 krpm to 243.8 krpm. 4 bar (150°C) oil feed pressure. Vertical eddy current sensor (compressor side).

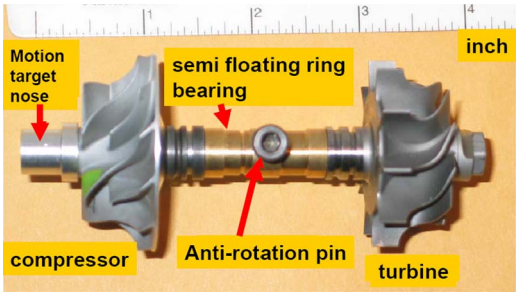

Fig. 1 Photograph of automotive turbocharger supported on semi-floating ring bearings

strength and lightweight materials (low inertia). For the experiments, the rotor was modified to include an aluminum sleeve at the compressor nose for measurement of shaft motions.

The semi-floating ring is a thick and long structural element made of a common material. The rotor and SFRB when installed in its casing give rise to an outer film and an inner film on both the compressor and turbine sides. A feed port on the casing supplies lubricant into the middle plane of the floating ring. On the other side, a pin locking the ring prevents its rotation. The inner diameter of the ring, at the location of the inner film land, is machined to form a four-pad bearing with deep axial grooves. The outer film bearing is a plain cylindrical geometry. Pressurized lubricant flowing from the feed port lubricates the ends of the fluid film lands, inner and outer.

Experiments recording the TC shaft motions were conducted with a commercial lubricant (5 W-30) supplied at a nominal inlet temperature of 150°C and feed pressures ranging from 1 to 4 bar. The lubricant has a nominal viscosity of 2.76 cPoise at the supply condition. The low lubricant viscosity and high supply temperature responds to severe environmental constraints required in modern passenger vehicle.

Calibrated imbalances (~0.1 gram mm) were inserted at the nose and back face of the turbine and compressor wheels and at the same angular location (in-phase). The imbalance distribution used denotes a most severe condition, as per the manufacturer considerations. In the experiments, a hot gas drove the turbine to a top speed of 243 krpm (4.0 kHz). Upon achieving a steady-state condition, the shaft motions at incremental rotor speeds were collected using a dynamic signal analyzer and a digital oscilloscope displaying the shaft orbital motions of the shaft at the compressor end. Fast Fourier transform (FFT) collected data has a maximum span of 6.4 kHz with frequency increments of 16 Hz (400 lines).

Figure 2 shows a waterfall of the recorded shaft vertical displacement for a 4 bar lubricant feed pressure as the rotor ramps up from 29.7 to 243.6 krpm. In the graph, the horizontal axis displays the frequency content of shaft motion, while the vertical axis denotes the amplitude of shaft motion. The shaft displacements are shown in dimensionless form, relative to the physical limit at the location of measurement. The continuous line denotes the synchronous frequency components. The test results show the dominance of subsynchronous frequency motions over the whole shaft speed range, 29.7 to 243 krpm. The shaft synchronous amplitude peaks at the lowest rotor speed and decreases slowly as the rotor speed increases. However, the shaft subsynchronous motions are of large amplitude with significant changes over the test speed range. A filter analysis of the collected data produces the components of synchronous and subsynchronous shaft motions. A discussion of the test results is given below, along with the numerical predictions.

Turbocharger Rotor and Semi-floating Ring Bearing

Figure 3 displays the finite element structural models for the rotor and semi-floating ring bearing, each represented by 45 and 4

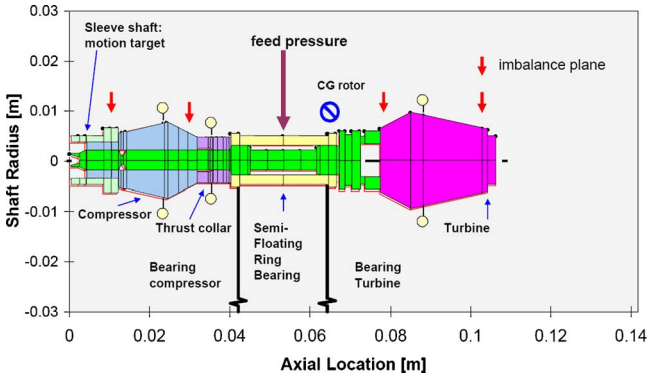

Fig. 3 Structural FE model of turbocharger rotor and semi-floating ring bearing. Location of mass imbalance planes noted.

elements, respectively. Inertia properties of the turbine, compressor, and thrust collar are included at the appropriate locations. Rap tests with the TC rotor hung from wires allow measuring its free-free mode natural frequencies and mode shapes. Two miniature piezoelectric, accelerometers, each 1 g in weight, were affixed on the rotor; one reference transducer remained at the turbine end, while the other roamed along the test rotor.

Figure 4 shows the measured and predicted free-free mode shapes. The first two natural frequencies recorded equal 1.07 and 4.77 kHz (±120 Hz), and the predicted values are 1.046 and 4.98 kHz, respectively. The agreement between predictions and measurements, both for natural frequencies and mode shapes, is excellent; thus lending validity to the structural rotor model developed. Note that rotor material properties at ambient conditions were used for the predictions.

Holt et al. [17,18] describe the integration of a rotordynamics computational program [20] to the thin film fluid flow model for prediction of the reaction loads in fully floating and semi-floating ring bearings. The rotordynamics finite element (FE) program, based on the component-synthesis method [21], predicts the linear stability (damped eigenvalues) and synchronous response of a rotor supported on bearings represented by linearized stiffness and damping force coefficients. The program, which also includes simple models for typical nonlinear mechanical elements, features a time transient numerical solution procedure for prediction of rotor responses to applied loads including shock and maneuver and initial conditions (blade simulations, for example).

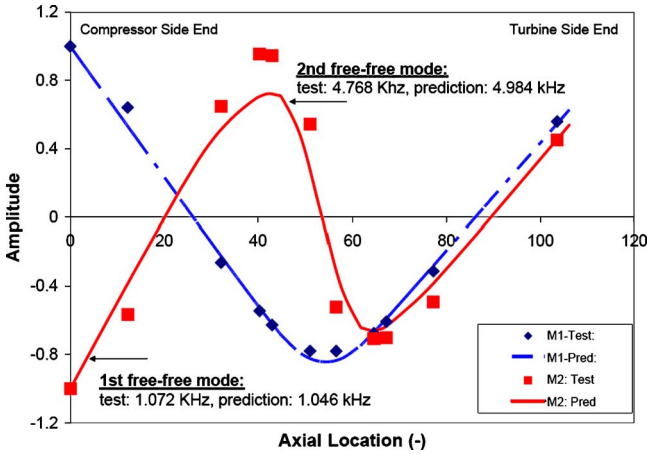

Fig. 4 Free-free mode shapes for turbocharger rotor—predictions and measurements at room temperature

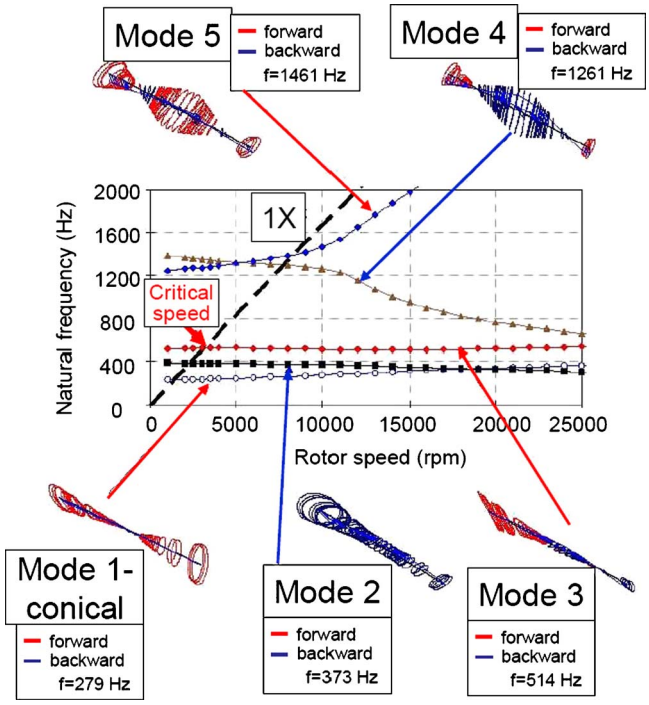

Fig. 5 Predicted damped natural frequencies versus shaft speed for test turbo charger rotor. Damped natural modes shown for shaft speed=100 krpm.

Kerth and San Andrés [19] detail the FE analysis of the laminar flow (Reynolds) equations for each fluid film along with a lumped parameter thermal model. The computational model for a (semi-) floating ring bearing predicts its forced performance as a function of the bearing geometry, applied load, shaft speed and lubricant properties, including shear thinning effects. The model does account for the temperature raise within each film, inner and outer, affecting the lubricant viscosity and operating clearances at each shaft speed.

The prediction of the nonlinear transient response of the TC rotor supported on the semi-floating ring bearings requires

(a) estimation of the static loads acting on each bearing;
(b) calculation of the equilibrium conditions for each film, namely, static eccentricity and attitude angle of journal and ring, temperature rise, and operating clearances and effective viscosities for both films in series;
(c) calculation of stiffness and damping force coefficients for the inner and outer films at the equilibrium position;
(d) integration of the actual SFRB operating conditions and side load into the rotordynamics program for prediction of system eigenvalues (damped natural frequencies and mode shapes) and the linear or nonlinear response due to a prescribed imbalance distribution.

Natural Frequencies and Associated Mode Shapes

Figure 5 depicts a map of the predicted damped natural frequencies versus shaft speed. The linear analysis relies on the specification of the stiffness and damping force coefficients for the inner and outer films at the turbine and compressor bearings. The graph also displays the rotor mode shapes at a shaft speed of 100 krpm. The rotor-bearing system critical speeds are noted on the intersection of the synchronous line (1*X*) with each of the natural frequencies. The lowest natural frequency (~200 Hz) corresponds with a rigid body conical (planar) mode shape. The other natural modes show increasing degrees of rotor bending, with

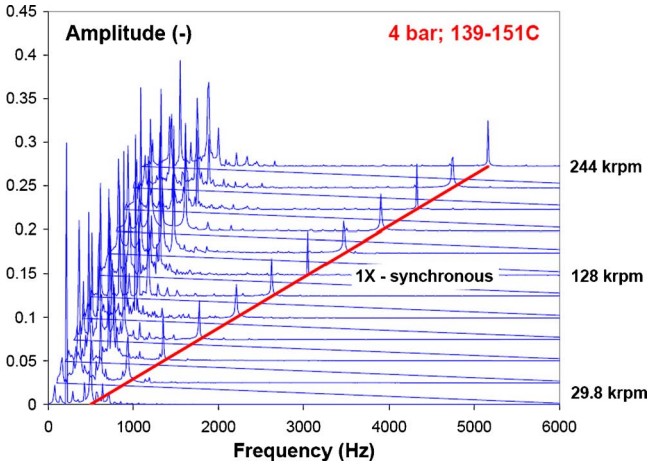

Fig. 6 Waterfall of predicted nonlinear (vertical) shaft motions at compressor end. Rotor range speed 29.7 to 244 krpm. 4 bar lubricant feed pressure. Amplitude refractive to maximum physical limit.

large motions at the compressor end, except for backward whirl mode 4. All modes are well damped (i.e., absence of instabilities) at all shaft speeds. The test data, on the other hand, show subsynchronous whirl motions over the whole speed range, thus demonstrating the limited applicability of the linear eigenvalue analysis.

Predictions of Shaft Motion and Comparisons to Test Data

The numerical integration of the nonlinear equations of motion for the rotor-SFRB system was conducted for the same test shaft speeds, 29.7 krpm (0.5 kHz) to 243 krpm (4.05 kHz), and lasting a sufficiently "long time" to warrant the prediction of a steady-state motion condition. A time step fixed at 78 μs renders a maximum frequency span equal to 6.4 kHz, similar to the signal analyzer setting recording the experiments. In most cases, the total time for integration of the governing equations lasts ~3/4 s, with only the "s-s" portion being analyzed giving a lowest frequency step of 6.25 Hz (2048 data points). In the measurements, a 16 Hz frequency step was used.

Post-processing mathematical software allows the comprehensive analysis of the nonlinear time response predictions to determine the amplitude and frequency content of the shaft motion over pre-selected time spans. FFTs are calculated with a sampling frequency of the same order as in the experiments, namely 12.5 Hz (1024 data points).

Figure 6 displays a waterfall graph of the predicted steady-state shaft motions at the compressor nose. The amplitudes are dimensionless relative to the physical limit of shaft displacement at the measurement plane. Note that, as with the experimental measurements, the predictions show persistent subsynchronous motions over the entire shaft speed range. Synchronous amplitude (1*X*) motions are but a small fraction of the total shaft motion at the compressor end. Figure 7 compares, at shaft speeds equal to 127 and 205 krpm, the FFTs of shaft motion acquired from the test data and the ones derived from the predicted nonlinear response. There is good agreement on the amplitudes of synchronous motion as well as on the location of the subsynchronous frequencies.

The waterfalls of shaft motion shown in Figs. 2 and 6 for tests and predictions, respectively, reveal a complex rotor response rich in subsynchronous activity. The test data and FFT predictions are filtered to capture the amplitude and frequency of the peak responses, including the synchronous components. The threshold amplitude for the analysis is 4% of the physical limit.

Figure 8 shows the total amplitude of shaft motion at the compressor end versus speed for both the test data and the nonlinear

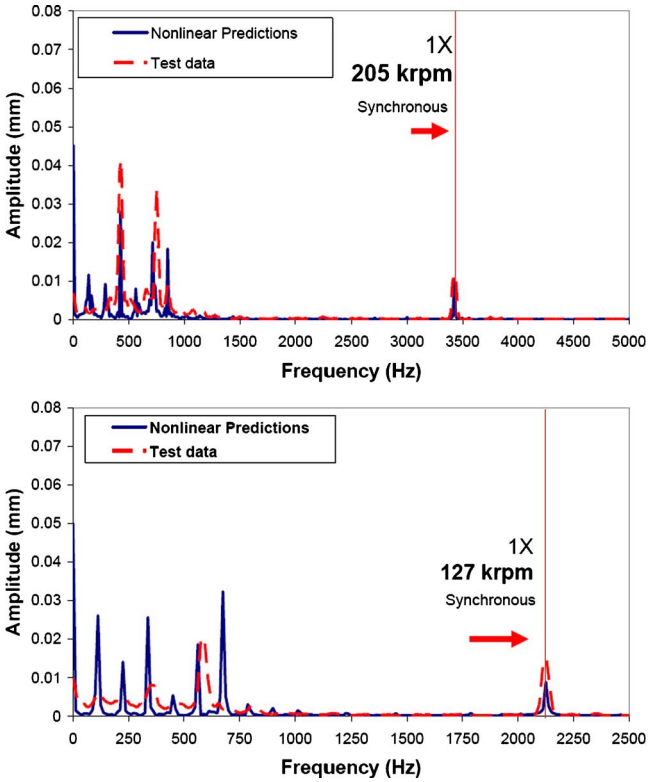

Fig. 7 FFTs of shaft motion at compressor end for rotor speeds equal to 127 krpm (bottom) and 205 krpm (top). Comparison of nonlinear predictions to test data. Note amplitudes at subsynchronous frequencies.

predictions. The size of the limit cycle orbit defines the total motion. The numerical data is analyzed over a time span that captures motions with a minimum frequency equal to 50 Hz. In general, the nonlinear predictions correlate very well with the test data at low and high shaft speeds. Predicted total motions are larger than test amplitudes in the speed range from 70 to 166 krpm, although well below the physical limit. An explanation of the differences follows later.

Figure 9 depicts the experimental and predicted amplitudes of synchronous (1*X*) motions versus shaft speed. The predictions shown are linear and nonlinear, with the nonlinear denoting the motion amplitudes synchronous with shaft speed as extracted

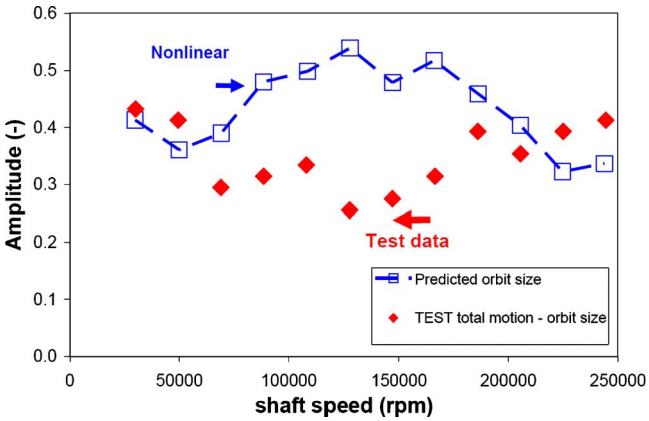

Fig. 8 Amplitudes of total motion at compressor end versus shaft speed. Comparisons between test data and nonlinear predictions. Oil feed pressure=4 bar (150°C).

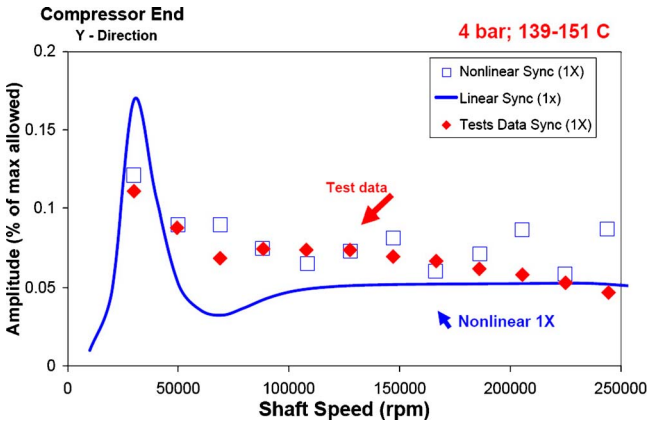

Fig. 9 Amplitudes of synchronous shaft motion versus shaft speed. Comparisons between test data and linear and nonlinear predictions. Oil feed pressure=4 bar (150°C).

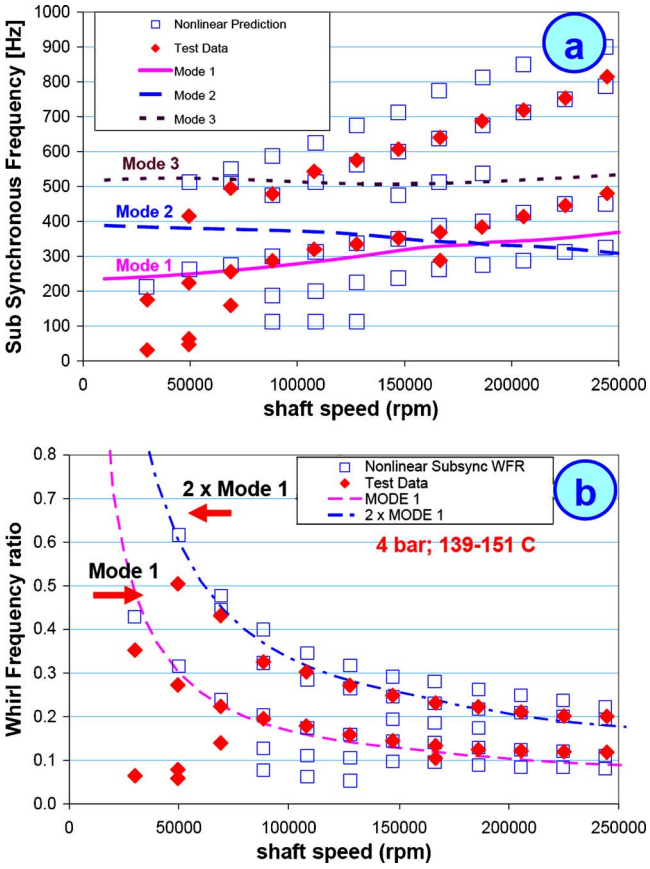

Fig. 10 (*a*) Whirl frequency of subsynchronous motions and (*b*) whirl frequency ratios versus shaft speed. Comparisons between nonlinear predictions and test data. Lines represent damped natural frequencies (linear analysis). Oil feed pressure=4 bar (150°C).

from the FFTs of the transient time response. The linear predictions, on the other hand, show the response to imbalance obtained with the (linearized) SFRB stiffness and damping coefficients for the inner and outer films. Recall that these force coefficients are calculated from small-amplitude perturbations of the journal and floating ring at their static equilibrium position. The rotordynamics software calculates the linear imbalance response very rapidly, while the nonlinear predictions need more computational time to be completed.

The nonlinear (synchronous response) predictions agree very well with the test data over the entire speed range. The linear response, on the other hand, predicts larger amplitudes at a lightly damped critical speed at 30.8 krpm (514 Hz) that represents rotor mode 3, i.e., the one with the compressor end "ringing" (see Fig. 5). Above the critical speed, the amplitudes of synchronous motion steadily decrease as the rotor operates well above any natural frequency. The rationale for the discrepancies between the measured data and nonlinear predictions are ascribed to the uncertainty in the (used) imbalance masses and their exact location in the rotor model. It is important to note that the linear analysis could be used effectively to predict the synchronous rotor response, in spite of the apparent nonlinearities.

In the analysis, a whirl frequency ratio (WFR) relates a whirl frequency to the shaft angular frequency (synchronous speed). Figure 10 depicts the frequency and WFR of the subsynchronous motions versus shaft speed in the top and bottom graphs, respectively. The test data shows two main subsynchronous frequencies that increase as the shaft speed raises. At the lowest shaft speeds, the whirl frequencies appear to coincide with the first two natural frequencies (modes 1 and 2). The nonlinear predictions for subsynchronous whirl frequencies agree very well with the measurements, albeit showing a third (unstable) higher subsynchronous frequency not evident in the tests. The WFRs decay steadily as the shaft speed increases; most notably, the second test whirl frequency is approximately two times the lowest WFR. The results demonstrate that the unstable shaft motions refer to excitations of the conical mode and its harmonics. The whirl frequencies tracking the shaft speed are particular to the operation of the nonrotating outer films (SFRB) acting as uncentralized squeeze film dampers.

Figures 11(*a*)–11(*c*) shows the amplitude of subsynchronous motions versus shaft speed (top graph) and whirl subsynchronous frequency (bottom graph). The continuous lines shown in the figures are hand-drawn and attempt to evidence characteristic trends mainly from the test data. The graphs display the intricacy of the test results and predictions. At a particular shaft speed, one or more subsynchronous amplitudes of motion are apparent. Conversely, subsynchronous amplitudes may also occur at more than one shaft speed. The results depicted intend to evidence trends of importance, for example persistent motions at a particular low frequency. The experiments and predictions indicate the largest motion occur at the lowest test rotor speed (29.7 krpm) with a frequency of ~200 Hz (WFR=0.35–0.43) coinciding with the (self-) excitation of the rotor conical mode. As the shaft speed increases to 127 krpm, the predicted and test derived amplitudes decrease steadily. For higher shaft speeds, there is a notable increase in subsynchronous motions with the test data showing larger amplitudes at the top shaft speed.

Figure 11(*b*) depicts the experimental amplitudes of subsynchronous motion to be confined in a narrow frequency range—200 to 800 Hz—which spans the first three natural modes of vibration (see Fig. 5). The hand-drawn continuous lines intend to show trends for the test data. For example, the largest amplitudes appear to correspond with the lowest mode of natural vibration and its 2nd harmonic (~200 Hz and 400 Hz) and decreasing in magnitude as the whirl frequency increases. The nonlinear predictions show similar trends, except for the appearance of the third whirl frequency in the range from 600 to 900 Hz.

Closure

Turbochargers are used in passenger vehicles to increase the overall efficiency and reduce emissions of internal combustion engines. Presently, automotive turbochargers operate at higher shaft speeds to increase their boosting power while using much lighter lubricants. Turbochargers using lubricated fluid film bearing show shaft motions with one or more subsynchronous fre-

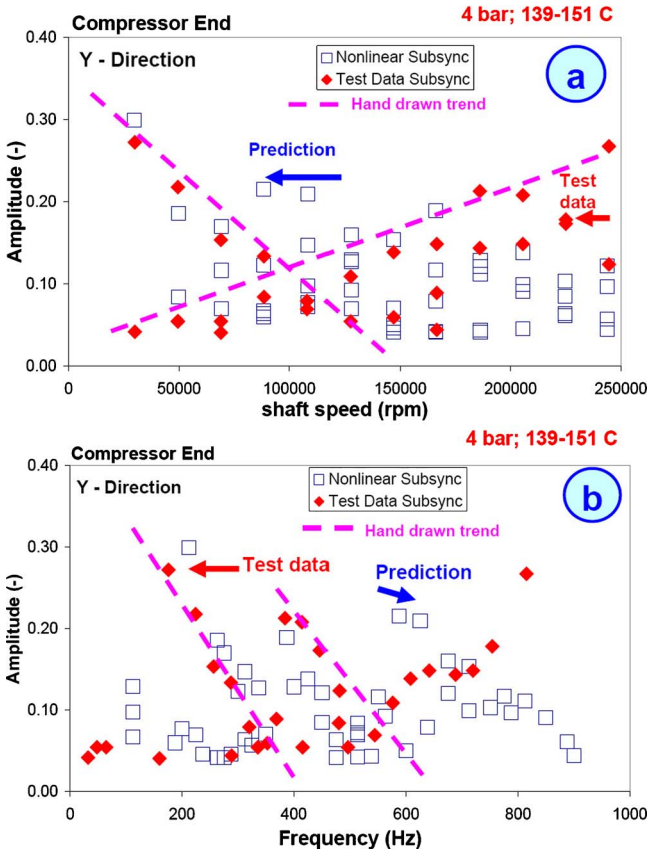

Fig. 11 Amplitudes of subsynchronous motions versus (*a*) shaft speed and (*b*) whirl frequency. Comparisons between nonlinear predictions and test data. Oil feed pressure=4 bar.

quencies, typically of large amplitude, and leading to limit cycle performance. Linear rotor dynamics analyses cannot reproduce the actual limit cycle motions.

In spite of the complexity of the measured and predicted rotor responses, i.e., rich in subsynchronous frequencies and amplitudes, the nonlinear results from the comprehensive predictive model replicate most of the trends, including amplitudes of limit cycle motion and subsynchronous whirl frequencies. The nonlinear predictions are in good agreement with the test data, thus validating the comprehensive computational model developed.

The usefulness of the predictive tool developed, however, can best be appreciated by performing an analysis of the myriad of other calculated variables that become available upon completion of the program execution. The current program delivers shaft motions at any station in the rotor, including the bearings, as well as the transmitted forces to the casing. Trends in shaft static motions, whirl orbits, lubricant exit temperatures, etc. are easily graphed for ready analysis. Even digital video clips of transient shaft motion can be generated automatically. The computational design tool effectively aids to design better turbocharger products with increased reliability and in less development time. Future publications will continue to detail further predictions and comparisons to test data.

Acknowledgment

The support of Honeywell Turbo Technologies is gratefully acknowledged, in particular for preparing the turbocharger test bed and collecting the comprehensive experimental results. Graduate student J.C.R. thanks Honeywell's engineering staff for their guidance and insight.

References

[1] Hill, H. C., 1958, "Slipper Bearings and Vibration Control in Small Gas Turbines," Trans. ASME, **80**, pp. 1756–1764.
[2] Trippett, R. J., and Li, D. F., 1983, "High-Speed Floating-Ring Bearing Test and Analysis," ASLE Trans., **27**(1), pp. 73–81.
[3] Macinnes, H., and Johnston, A., 1982, "Comparison of Power Loss Between Full Floating and Semi-Floating Turbocharger Bearings," *Proceedings of IMechE Conference on Turbocharging and Turbochargers*, London, Paper C46/82, pp. 157–164.
[4] Tatara, A., 1970, "An Experimental Study of the Stabilizing Effect of Floating-Bush Journal Bearings," Bull. JSME, **13**(61), pp. 859–863.
[5] Holmes, R., Brennan, M. J., and Gottrand, B., 2004, "Vibration of an Automotive Turbocharger–A Case Study," *Proceedings of the 8th International Conference in Vibrations and Rotating Machinery*, IMechE Wales, UK, Paper C623/011/2004, pp. 445–455.
[6] Tanaka, M., and Hori, Y., 1972, "Stability Characteristics of Floating Bush Bearings," Trans. ASME, **94**, pp. 248–259.
[7] Tanaka, M., 1996, "A Theoretical Analysis of Stability Characteristics of High Speed Floating Bush Bearings," *Proceedings of the 6th International Conference on Vibrations in Rotating Machinery*, IMechE Conference Transaction 1996-6, London, Paper C500/087/96, pp. 133–142.
[8] Tanaka, M., 2002, "A Parametric Study of the Stability of High-Speed Floating Bush Journal Bearings," *Proceedings of the 6th IFToMM International Conference on Rotor Dynamics*, Sydney, Australia, 2, pp. 549–555.
[9] Rohde, S. M., and Ezzat, H. A., 1980, "Analysis of Dynamically Loaded Floating-Ring Bearings for Automotive Applications," ASME J. Lubr. Technol., **102**, pp. 271–277.
[10] Li, C. H., and Rohde, S. M., 1981, "On the Steady State and Dynamic Performance Characteristics of Floating Ring Bearings," ASME J. Lubr. Technol., **103**, pp. 389–397.
[11] Li, C., 1982, "Dynamics of Rotor Bearing Systems Supported by Floating ring Bearings," ASME J. Lubr. Technol., **104**, pp. 469–477.
[12] Sahay, S. N., and Thouvenin, D., 1993, "Turbocharger Noise, Generating Mechanisms and Control," Noise, **93**, pp. 269–277.
[13] Sahay, S. N., and LaRue, G., 1996, "Turbocharger Rotordynamic Instability and Control," *Proceedings of the 8th Workshop on Instability in Rotating Machinery*, Texas A&M University, College Station, TX, pp. 1–11.
[14] Gjika, K., 2003, "Turbocharger Bearing Systems Technology," Garrett Booster Magazine, March, pp. 6–11.
[15] Naranjo, J., Holt, C., and San Andrés, L., 2001, "Dynamic Response of a Rotor Supported in a Floating Ring Bearing," *Proceedings of the 1st International Conference in Rotordynamics of Machinery*, ISCORMA1, Lake Tahoe, NV, Paper 2005.
[16] Holt, C., San Andrés, L., Sahay, S., Tang, P., LaRue, G., and Gjika, K., 2003, "Test Response of a Turbocharger Supported on Floating Ring Bearings–Part I: Assessment of Subsynchronous Motions," *Proceedings of the 19th Biennial Conference on Mechanical Vibration and Noise*, Chicago, IL, ASME Paper DETC 2003/VIB-48418.
[17] Holt, C., San Andrés, L., Sahay, S., Tang, P., LaRue, G., and Gjika, K., 2003, "Test Response of a Turbocharger Supported on Floating Ring Bearings–Part II: Comparisons to Nonlinear Rotordynamic Predictions," ASME Paper No. DETC 2003/VIB-48419.
[18] Holt, C., San Andrés, L., Sahay, S., Tang, P., LaRue, G., and Gjika, K., 2005, "Test Response and Nonlinear Analysis of a Turbocharger Supported on Floating Ring Bearings," ASME J. Vibr. Acoust., **127**, pp. 1–9.
[19] Kerth, J., and San Andrés, L., 2004, "Thermal Effects on the Performance of Floating Ring Bearings for Turbochargers," Proc. Inst. Mech. Eng., Part J: J. Eng. Tribol., **218**(5), pp. 437–450.
[20] XLTRC^2 Rotordynamics Software Suite v. 2, 2002, Turbomachinery Laboratory, Texas A&M University, College Station, TX.
[21] Nelson, H., and Meacham, W., 1981, "Transient Analysis of Rotor-Bearing System Using Component Mode Synthesis," ASME Paper No. 81-G7-10.